The International Journal of Advanced Manufacturing Technology (2018) 96:3437–3447
https://doi.org/10.1007/s00170-018-1833-0

ORIGINAL ARTICLE

Prediction and experimental validation of temperature rise in ductile mode end milling of soda-lime glass

Mst. Nasima Bagum[1] · Mohamed Konneh[1] · A. K. M. Nurul Amin[1]

Received: 27 November 2017 / Accepted: 22 February 2018 / Published online: 6 March 2018

Abstract
The suitable thermal, chemical, and corrosion resistance properties of glass make it possible to be used in a wide variety of product manufacturing, like lenses, mirrors, mold, semiconductor, biomedical, optical, and micro-electronics. However, machining of glass like any brittle material has big challenges owing to its inherent brittleness. Ductile mode machining is known to promote the material removal from a brittle material in ductile manner rather than by brittle fracture. In high-speed machining, the thermal softening effects can enhance flexibility in ductile machining of brittle materials. In this paper, an analytical model is developed to predict the amount of temperature generated in the immediate next removable layer (INRL) of the soda-lime glass work piece per unit depth of cut $\Delta\overline{T}_{\mathrm{INRL}}$ based on fundamental micro-machining principle and material physical properties. The model incorporates the effects of cutting speed, feed rate, strain rate, and thermal softening effect. The simulation and experimental results showed that at high cutting speed, glass softening can be achieved by adiabatic heating in order to facilitate ductile machining. The amount of adiabatic heating can be controlled by predicting the amount of the $\Delta\overline{T}_{\mathrm{INRL}}$.

Keywords High-speed milling · Soda-lime glass · Uncut chip thickness · Shear stress · Cutting zone temperature · Analytical model

1 Introduction

Glass is used in electronic industries as well as in health affairs like optics and biomedical industries [1]. Soda-lime glass is widely used in windowpanes, chemical apparatus, camera lens, micro-gas turbines, etc. It is relatively an inexpensive material [2]. However, soda-lime glass, known as difficult-to-cut materials, imposes significant challenges in machining due to its brittle nature. Over the decades, researchers focused on the assessment of plastic deformation phenomenon of brittle materials like glass and ceramics to fulfill the request for their widespread applications.

✉ Mst. Nasima Bagum
nasimaanam@gmail.com

[1] Department of Manufacturing and Materials Engineering, Kulliyyah of Engineering, International Islamic University Malaysia, Jalan Gombak, 53100 Kuala Lumpur, Malaysia

Researchers have mainly focused on the ductile-brittle transition point during turning and grinding of brittle materials. In ductile regime machining (DRM), the size of the critical stress field as well as brittle-ductile transition point is mainly governed by the critical value of un-deformed chip thickness (UCT). Bifano et al. [3] defined critical UCT as a function of material intrinsic properties. Bifano et al. [3] developed a model for indentation on brittle materials but the cutting mechanics and thermal softening effects, involve in practical machining, were not incorporated. In case of single-point cutting inserts, extensive research has been done mainly focused on the application of high hydrostatic pressure and large negative rake angles induced by uncut chip thickness and tool edge radius relation. Researchers [4, 5] commented on the relationship between tool edge radius, UCT, and the work material brittleness. In this situation, the UCT should be smaller than the tool edge radius and the tool cutting edge radius should be small enough on a nano-scale for nano-machining [5]. Furthermore, the maximum value of cut-

ting edge radius should be at nano-scale for machining materials of high brittleness and at micro-scale for comparatively less brittle materials [4]. Nevertheless, in these conventional processes due to brittle nature of work piece, the achievement of ductile machining was restricted at submicron scale cutting parameters considering the probability of crack generation and breakage.

Although milling is a versatile process for machining three-dimensional shapes and free forms, DRM with multipoint cutting tool is still an emerging area of research. In case of end milling operation, the critical feed per edge and axial depth influences the DRM. At a relatively low cutting speed (less than 10 m/min), fracture-free surface was achieved at high radial depth of cut below 0.875 μm feed per edge [6]. However, the machining mode was transited from ductile to brittle due to the chipping or breakage of the cutting edge due to excessive wear. At low value of the cutting speed range (0.2–0.62 m/s), Zhao et al. [7] showed that both feed per edge and axial depth of cut have major influence while cutting speed has less impact on the ductile regime micro-end slot milling of soda-lime glass. Hence, at low cutting speed, the cutting parameters to achieve DRM with multipoint cutting tool are also limited to submicron scale. Therefore, high material removal rate (MRR) in glass machining is yet to achieve.

In order to achieve higher MRR in ductile machining and to attain micro-finished surface, researchers worked on experimental technique. For instance, using ultrasonic vibration [8], the friction between the tool chip interface is reduced, thereby critical chip thickness improved significantly and MRR also increased. Consequently, analytical model development [9] and performance upgradation of vibration-assisted machining [10] were navigated. For thin glass machining, researchers tried to apply abrasive water jet machining [11, 12], electrochemical discharge machining [13], electrolytic in process dressing, and laser machining. In laser-assisted DRM machining, intense heat generated using laser [14, 15] was utilized to decrease material yield strength, which enabled ductile/plastic deformation rather than brittle fracture. However, each of the process has some limitations and required huge capital investment. This necessitated the desire to explore the effects of high cutting speed coupled with ductile mode machining criteria in milling soda-lime glass. Researchers have demonstrated that at higher cutting speed, the critical chip thickness was higher due to thermal softening [16]. In case of machinable glass ceramic, the analytical model proved that with the increase of spindle speed, surface roughness decreased [17]. Amin and his co-authors [18] achieved ductile mode machining at axial depth of cut between 1.558 and 51.943 μm, while end milling of soda-lime glass at high cutting speed (10.47 m/s) and feed rate 20 mm/min. Soda-lime glass experienced material softening under loading at elevated temperatures [19]. This material softening has influence on the mechanical properties such as fracture toughness [19], hardness [20], and Young's modulus. At elevated temperature, soda-lime glass's brittleness index is decreased by reducing its hardness to toughness ratio. It is also revealed that around glass transition temperature, fracture toughness of soda-lime glass increased (necessary for ductile machining) and glass transition temperature also varies depending on the loading rate [21]. In high-speed machining, the relationship between machining parameters and the change of thermo-mechanical properties of the work material, due to adiabatic thermal softening in shear zone induced by machining, would facilitate the achievement of ductile mode that is yet to establish.

In view of understanding the basic phenomenon of achievement of ductile regime at high cutting speed, the objective of this paper is to develop an analytical model to predict the amount of temperature generated in immediate next removable layer (INRL) of soda-lime glass by using fundamental micro-machining principle and material physical properties, which incorporates the effects of cutting speed, feed rates, strain rate, material strength, and thermal softening effect.

2 Model development

The assumption of the paper is that due to ductile mode cutting of glass, it is then possible to use Johnson and Cook (JC) model [22] (usually used for ductile metals), and slip-line field (also assuming plastic flow) in modeling the micro-cutting of soda-lime glass. For ductile mode cutting, in this research, cutting tool edge radius is chosen at micro-level and greater than uncut chip thickness. In order to apply the shear plane model, an equivalent sliding plane for chip on the cutting tool surface is anticipated. This plane detects the effective rake angle α_e and can be well defined by a plane tangent to the edge radius at a distance from the machined surface to the uncut chip thickness as shown in Fig. 1.

Hence, instantaneous effective rake angle $\propto_e$ is possible to articulate depending on the ratio of uncut chip thickness and cutting tool edge radius by the following expression [9, 23, 24].

$$\propto_e = \begin{cases} \sin^{-1}\left(\frac{t_1}{r_e} - 1\right) & \text{when}\left(\frac{t_1}{r_e} \le 1 + \sin\propto_n\right) \\ \propto_n & \text{when}\left(\frac{t_1}{r_e} > 1 + \sin\propto_n\right) \end{cases} \quad (1)$$

where$\propto_n$, r_e, *and*$\propto_e$ represents the nominal rake angle, cutting edge radius, and effective rake angle. Therefore, instantaneous

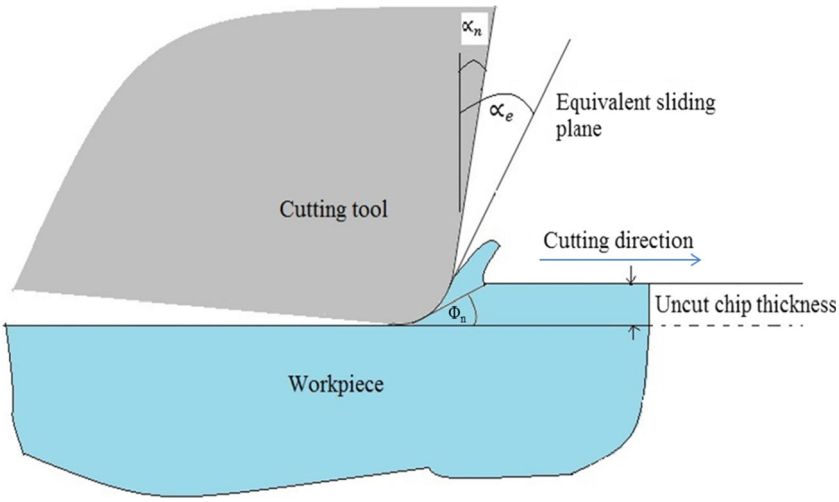

Fig. 1 An equivalent sliding plane and rake angle due to edge radius

effective shear angle ϕ_n can be quantified by considering the instantaneous rake angle $\propto_e$ as in Eq. (2) [25].

$$\phi n = \tan^{-1}\left(\frac{r_c \cos \propto_e}{1 - r_c \sin \propto_e}\right) \tag{2}$$

The chip thickness ratio or cutting ratio, r_c, is the ratio of the un-deformed chip (t_1) to the cut chip thickness (t_2). In case of micro-machining, the chip thickness ratio known as cutting ratio varies from 0.29 to 0.36 [26]. Henceforth, cutting ratio of soda-lime glass is assumed to vary from 0.29 to 0.4.

2.1 Average temperature rise in the INRL of the work piece per unit depth of cut

The chip formation takes place in the plastic zone; the chips run from the cutting edge of the tool to the tool chip interface. According to Oxley's energy partition function, the average temperature rise of the chip per unit depth of cut ($\Delta\overline{T}$), due to shearing in orthogonal cutting operation, is expressed by Eq. (3) [27].

$$\Delta\overline{T} = \dot{Q_S}\frac{1-\mathcal{X}}{\rho.c_c.t_1.V_w} \tag{3}$$

where $\dot{Q_S}$, $\mathcal{X}$, ρ, c_c, t_1, and V_w are the heat generation per unit depth of cut in primary shear zone, fraction of shearing flux conducted into the work piece, material density, specific heat capacity of chip, uncut chip thickness, and cutting velocity, respectively. Here, $(1-\mathcal{X})$ is the fraction of shearing flux entering into the chip.

As soda-lime glass has low thermal conductivity, it is assumed that fraction of shearing flux $(\mathcal{X})$ conducted into the

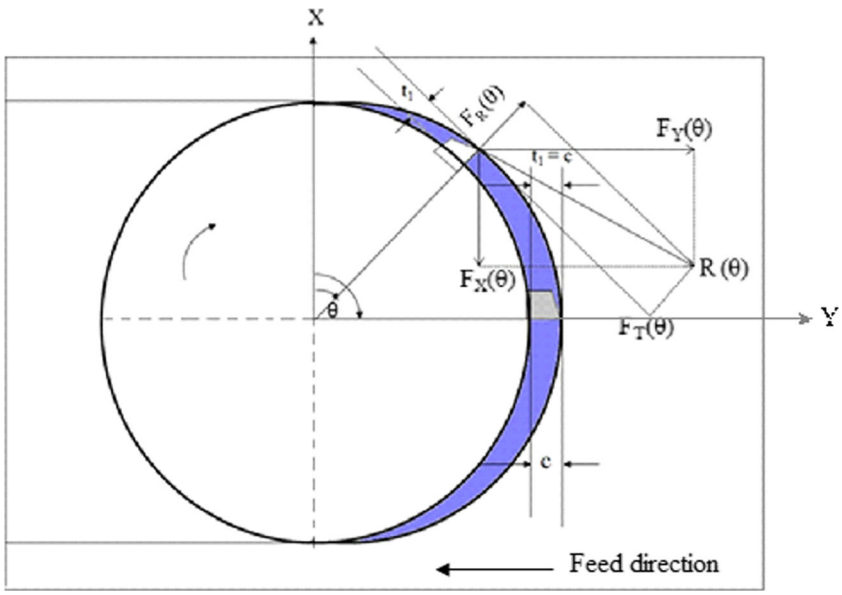

Fig. 2 Geometry of end milling, force component acting on the cutting edge, and work piece contact point

work piece is confined in the INRL, the shaded area of the work material in Fig. 2. Hence, due to the effect of shearing, the average temperature rise in the INRL of the work piece per unit depth of cut can be expressed by the following expression.

$$\Delta\overline{T}_{\mathrm{INRL}} = \dot{Q_S}\frac{\mathcal{X}}{\rho.c_c.t_1.V_w} \tag{4}$$

This predictive model of temperature is based on the following physical mechanism of material removal. If the temperature rises in the INRL ($\Delta\overline{T}_{\mathrm{INRL}}$), due to shearing, can be reached nearby the glass transition temperature, material removal will take place through localized plastic deformation. As fracture toughness of soda-lime glass is high enough around glass transition temperature [19, 21].

The fraction of shearing flux conducted into the work piece $\mathcal{X}$ can be evaluated with the following experimentally evaluated empirical equation [27].

$$\mathcal{X} = 0.5{-}0.35\ log_{10}(R_t.\tan(\phi_n)) \quad for\ 0.004{\le}R_t.\tan(\phi_n){\le}10 \tag{5}$$

$$\mathcal{X} = 0.3{-}0.15\ log_{10}(R_t.\tan(\phi_n)) \quad for\ \ R_t.\tan(\phi_n) > 10 \tag{6}$$

where ϕ_n is the instantaneous effective shear angle and thermal number R_t is a non-dimensional parameter.

In end milling, the uncut chip thickness t_1 depends on the cutter rotation angle θ or angular position of cutter and feed per tooth c by the relation $t_1 = c\ \sin(\theta)$ as shown in Fig. 2. Hence, thermal number depends on material properties such as material density ρ, thermal conductivity k_c, and specific heat capacity c_c, and chip load can be expressed by

$$R_t = \frac{t_1.\ V_w}{\zeta} = \frac{t_1.\ V_w.\rho.c_c}{k_c} = \frac{c\sin(\theta).V_w.\rho.c_c}{k_c} \tag{7}$$

The heat transmitted to the work materials cannot be more than the total energy generated, that means a negative influx of the heat into the shear plane is not possible, hence it is assumed that $(0{\le}\mathcal{X}{\le}1)$.

The amount of heat produced in primary shear zone depends on the shear stress in shear plane (τ),cutting velocity (V_w), nominal rake angle (α_n), and shear angle (ϕ_n). In orthogonal cutting, it is assumed that the chip is serrated from the work piece at an infinitely thin shear plane (primary shear zone). At that point, the amount of heat produced per unit depth of primary shear zone $\dot{Q_S}$ can be defined by Eq. (8) [28].

$$\dot{Q_S} = \frac{\tau.t_1.V_w.\cos(\alpha_n)}{\sin(\phi_n)\cos(\phi_n{-}\alpha_n)} \tag{8}$$

In high-speed machining, the work material is exposed to huge amount of strain, strain rate, and temperature. In addition, it is also considered that the amount of strain, strain rate, and temperature influences the chip formation process during DRM. Therefore, in this research, JC constitutive model [22] is considered applicable to predict flow stress of brittle materials such as soda-lime glass. Hence, the flow stress σ_f including the effect of strain hardening, strain rate, and thermal softening is given by the Eq. (9) [26].

$$\sigma_f = (A + B(\varepsilon)^n)\left(1 + C\ ln\left(\frac{\dot{\varepsilon}}{\dot{\varepsilon}_0}\right)\right)\left(1{-}\left(\frac{T{-}T_r}{T_{m{-}T_r}}\right)^m\right) \tag{9}$$

where A, B, C are the yield strength, strain hardening coefficient, and strain rate coefficient of the work material. The hardening and softening exponents are represented by n and m respectively. ε is equivalent plastic strain and $\dot{\varepsilon}$ is equivalent plastic strain rate and $\dot{\varepsilon}_0$ is reference plastic strain rate which is equal to 1.0 S^{-1}. Amount of the average temperature T at the shear plane can be estimated by integrating the following expression [29].

$$\int_{T_r}^{T_{av}} \frac{\rho.c_c}{\left(1{-}\left(\frac{T{-}T_r}{T_m{-}T_r}\right)^m\right)}\,dT = \beta(A + B(\varepsilon)^n)\left(1 + C\ ln\left(\frac{\dot{\varepsilon}}{\dot{\varepsilon}_0}\right)\right) \tag{10}$$

where β represents the proportion of shear deformation energy causing the temperature rise (appearing as sensible heat) and is assumed as 0.9. T_m and T_r are the material melting temperature and initial room temperature respectively. Using von Mises yield criteria, at shear plane, the amount of shear flow at plane strain condition τ_{sf} is

$$\tau_{sf} = \frac{1}{\sqrt{3}}(A + B(\varepsilon)^n)\left(1 + C\ ln(\frac{\dot{\varepsilon}}{\dot{\varepsilon}_0})\right)\left(1{-}\left(\frac{T{-}T_r}{T_{m{-}T_r}}\right)^m\right) \tag{11}$$

The equivalent plastic strain (ε) and strain rate ($\dot{\varepsilon}$) in the main shear plane can be given by Eqs. (12) and (13), respectively [27].

$$\varepsilon = \frac{\cos(\alpha_n)}{2\sqrt{3}\sin(\phi_n)\cos(\phi_n{-}\alpha_n)} \tag{12}$$

$$\dot{\varepsilon} = \frac{2\ V_w\cos(\alpha_n)}{\sqrt{3}(t_1)\cos(\phi_n{-}\alpha_n)} \tag{13}$$

Arranging Equations 1, 2, 4, 5, 8, 11, 12, and 13, the final equation to calculate $\Delta\overline{T}_{\mathrm{INRL}}$, due to shearing based on Oxley's energy partition function and combined material model, is given by Equation (14). In order to validate

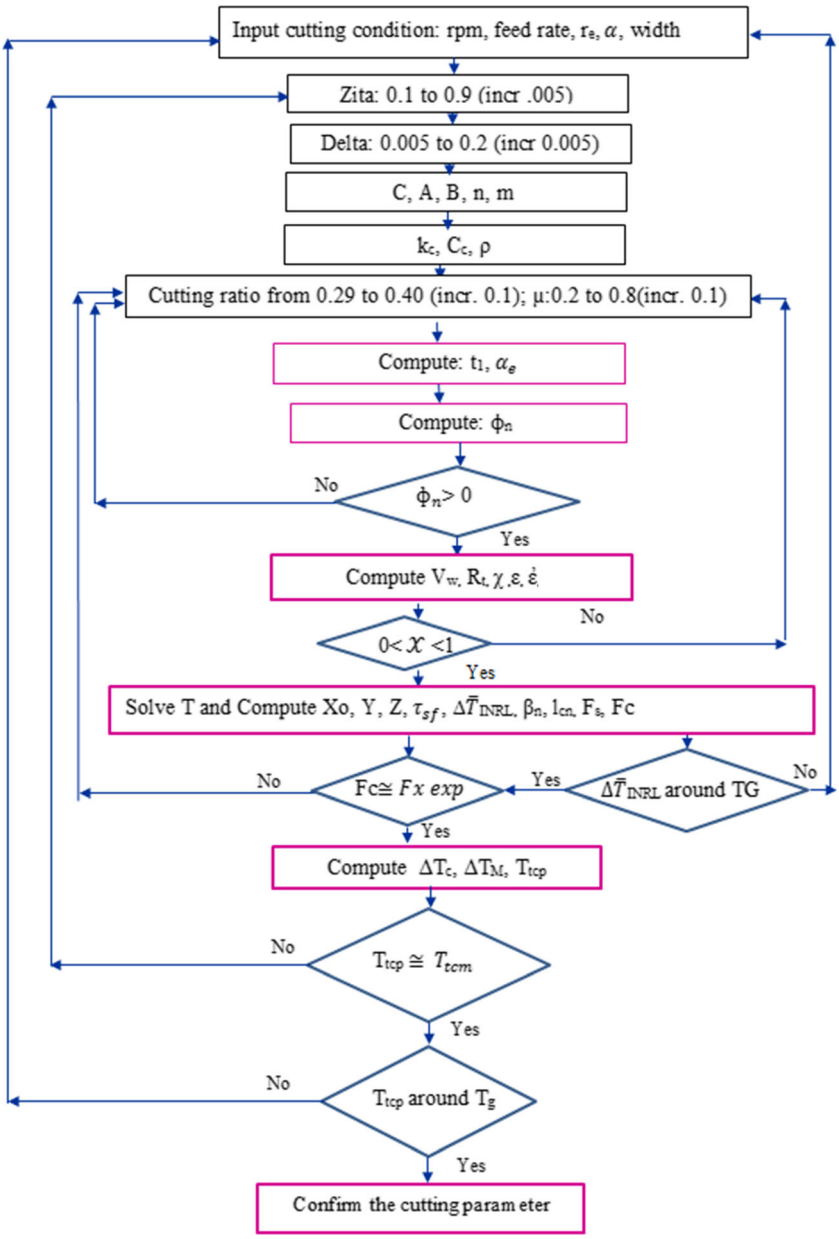

Fig. 3 The method of computing the analytical model's temperature using MATLAB

Equation (14), the average temperature at the tool chip interface T_{tcp} is also predicted as illustrated in section 2.2.

$$\Delta\bar{T}_{INRL} = \left(\frac{\tau_{sf}.t_1.V_w.\cos(\alpha_n)}{\sin(\phi_n)\cos(\phi_n-\alpha_n)}\right)\left(\frac{\chi}{\rho.c_c.t_1.V_w}\right) = \left(\frac{\tau_{sf}.\cos(\alpha_n)}{\sin(\phi_n)\cos(\phi_n-\alpha_n)}\right)\left(\frac{\chi}{\rho.c_c.}\right) \quad (14)$$

Table 1 Material constants used for simulation [32, 33]

Material constant	Value
Yield strength, A	69 MPa [34]
Strain hardening coefficient, B	150 MPa [35]
Materials strain hardening exponents, n	0.3
Strain rate coefficient, C	0.035 [36]
Reference plastic strain rate, $\dot{\varepsilon}_0$	$1S^{-1}$
Material melting temperature, T_m(°C)	1400 °C
Room temperature, T_r (°C)	25 °C
Material softening exponent, m	0.997

2.2 Average temperature at the tool chip interface

The chip formation takes place in plastic zone and the chips flow from the cutting edge of the tool to the tool chip interface; hence, temperature at the tool chip interface, T_{tcp}, can be predicted based on the initial work temperature; T_r, the value of average temperature rise of the chip per unit depth of cut in primary shear zone; $\Delta\overline{T}$, maximum temperature rise in the chip at the tool chip interface ΔT_M by Eq. (15).

$$T_{tcp} = T_r + \Delta\overline{T} + \psi\,\Delta T_M \quad (15)$$

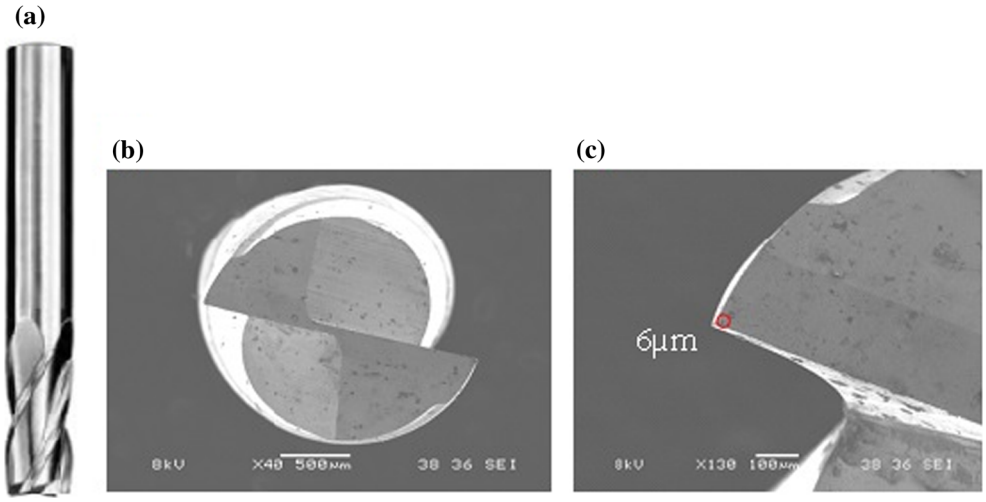

Fig. 4 **a** Milling tool. **b** Cutting edge. **c** Edge radius

The variation of temperature along the tool chip interface temperature is considered by the term ψ, where $\psi = (0 < \psi \leq 1)$.

Following the procedure similar to Eq. 14, the average temperature rise of the chip per unit depth of cut in primary shear zone $\Delta\overline{T}$ can be expressed by Eq. (16).

$$\Delta\overline{T} = \left(\frac{\tau_{sf}.\cos(\alpha_n)}{\sin(\phi_n)\cos(\phi_n - \alpha_n)}\right)\left(\frac{1-\mathcal{X}}{\rho.c_{c.}}\right) \tag{16}$$

Assuming rectangular plastic zone, the relation between average temperature (ΔT_c) and maximum temperature (ΔT_M) rise in the chip that occurs at the tool chip interface can be expressed by Eq. (17) [30]. The value of δ depends on the strain at the tool chip interface usually varied from 0.005 to 2, i.e., δ= .005 to 2. The tool chip contact length l_{cn} is calculated using Eq. (18) [31], where friction angle is assumed depends on the value of coefficient of friction between tool rake face and work piece, μ. In HSM usually, μ varies from 0.2 to 0.8. Hence, in the current study, the value of coefficient ranges from 0.2 to 0.8 as the machining is conducted using high speed.

$$\log_{10}\left(\frac{\Delta T_m}{\Delta T_c}\right) = 0.06 - 0.195\,\delta\left(\frac{R_t t_2}{l_{cn}}\right)^{1/2} + 0.5\log_{10}\left(\frac{R_t t_2}{l_{cn}}\right) \tag{17}$$

$$l_{cn} = \frac{2.t_1\,\sin(\phi_n + \beta_n - \alpha_n)}{\cos(\beta_n).\sin(\phi_n)} \tag{18}$$

With the assumption of uniform stress distribution on the shear plane, the cutting force F_c is expressed as Eq. (19), where the shear force F_s is found from shear stress τ_{sf} and shear plane area A_s relation as in Eq. (20). Therefore, average temperature in the chip at the tool chip interface ΔT_c is calculated using Eq. (21), where F_c is the cutting force in velocity direction and w is the chip width.

$$Fc = \frac{F_s\cos(\beta_n - \alpha_n)}{\cos(\phi_n + \beta_n - \alpha_n)} \tag{19}$$

$$F_s = \tau_{sf}.A_s = \tau_{sf}\mathrm{w}.\frac{t_1}{\sin(\phi_n)} \tag{20}$$

$$\Delta T_c = \frac{F_c\,sin\,\beta_n sin\phi_n}{\cos(\beta_n - \alpha_n).\rho.c_{c.}\,t_1\,w\cos(\phi_n - \alpha_n)} \tag{21}$$

3 Simulation and model validation

To simulate the analytical model to predict the amount of $\Delta\overline{T}_{\mathrm{INRL}}$ induced due to the end milling of soda-lime glass, a computer program in MATLAB (R2014a) was developed. The method of computation of the machining condition is specified in Fig. 3. The simulation was carried out based on the data of cutting tool geometry, soda-lime glass properties, and the material constants (given in Table 1).

4 Experimental details

4.1 Set up

End milling was conducted with a tungsten carbide cutter of 4 mm diameter, having two flutes. The grain size of the carbide was 0.6 μm. The uncoated tool flat end mill shown in Fig. 4 was chosen to get the heating benefits during cutting.

Table 2 Soda-lime glass properties*

Properties	Value
Material density, ρ (kg/m^3)	2500
Specific heat capacity of chip, c_c (j/kg/°C)	800
Thermal conductivity, k_c (W/m-°C)	0.96

*(http://www.makeitfrom.com)

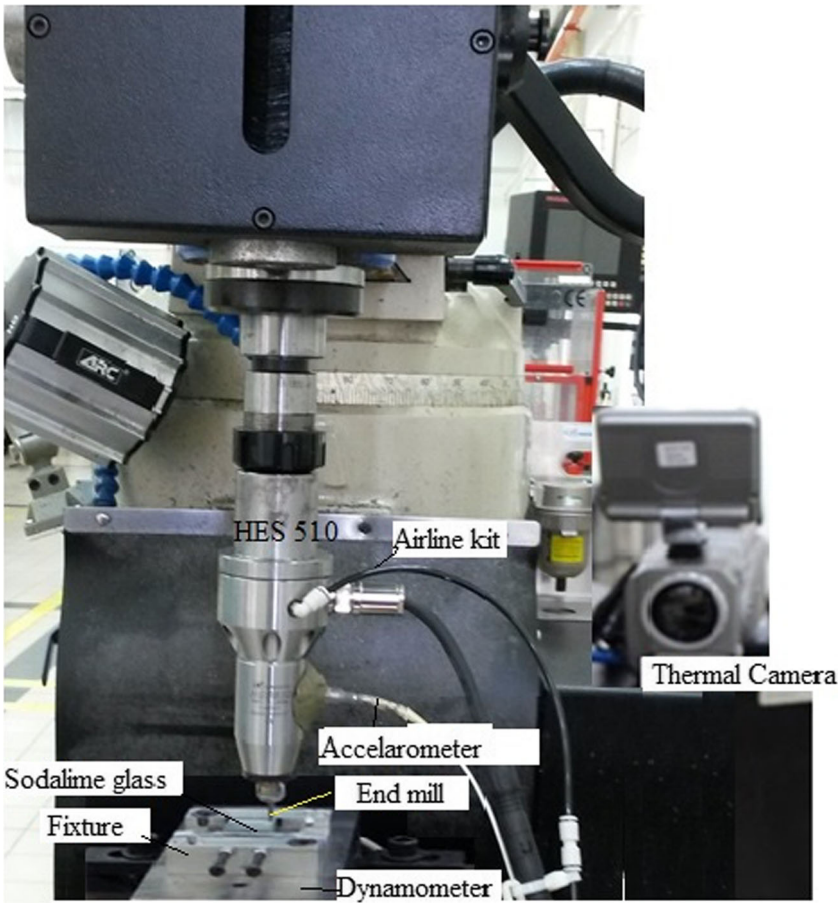

Fig. 5 Experimental setup

The cutting edge radius was at micro-scale (6 μm), rake angle −5°, and helix angle 35°. The square pieces of soda-lime glass with the dimension of 25 × 25 × 5 mm were used. The properties of soda-lime glass are given in Table 2. The workpiece was fixed to aluminum fixture with a special screw arrangement. The fixture was screwed to the dynamometer Kistler 9257B and dynamometer on a machine table by means of chuck. The end milling operations were carried out on a CNC Milling Machine (Model ECM 1) powered by a 2.2 KW motor. A Nakanishi Incorporation's HES 510 high-speed milling attachment was installed directly into its main spindle to upgrade this machining center to a high-speed machine. With this ultra-precision high-speed spindle, it is possible to get maximum 50,000 rpm (min^{-1}) and 250 W power output. The HES 510 high-speed spindle is externally controlled by the electric control unit (ECU) E3000. Nakanishi (AL-0201) airline kit supplies the clean air from the external compressed air line to the electronic control unit. The tool chip contact point temperatures T_{tcm} were recorded using the thermal camera Thermo Pro TP8 during cutting. A snapshot of the machining setup is shown in Fig. 5. Table 3 shows the combinations of cutting parameters used to conduct experiment in dry condition and simulation as well.

4.2 Data acquisition

After machining, the condition of machined surface was examined using optical microscope. The machined surface roughness was measured using Veeco Wyko Profiling system Microscope model NT110. The surface texture and chip morphology was studied using a scanning electron microscope (SEM), JSM-5610, and JBM-6700F, respectively.

5 Results and discussions

Comparative results of simulation and experimentation at different combinations of cutting parameters are

Table 3 Cutting parameters used to conduct experiment

Run no.	1	2	3	4	5
Spindle speed, rpm	40,000	30,000	30,000	30,000	40,000
(Cutting speed, m/s)	(8.37)	(6.28)	(6.28)	(6.28)	(8.37)
Feed rate, mm/min	10	10	20	30	30
(Uncut chip, t_1 μm)	(0.13)	(0.17)	(0.34)	(0.50)	(0.38)
Depth of cut, μm	50	40	40	40	30

Table 4 Comparison of simulated and experimental results

Run no.	Cutting parameters				Response				Simulation temperature $\Delta\overline{T}_{INRL}$ (°C)
	Spindle speed (rpm)	Cutting speed (m/s)	Feed rate (mm/min)	Depth of cut (μm)	Cutting Force F_x (*N*)		Average temperature at the tool chip interface (°C)		
					Experimental	Simulation	Experimental T_{tcm}	Simulation T_{tcp}	
1	40,000	8.37	10	50	43.94	41.91	587.56	583.78	566.33
2	30,000	6.28	10	40	50.85	50.89	520	520.3	541.21
3	30,000	6.28	20	40	51.98	51.62	736	731.03	697.25
4	30,000	6.28	30	40	54.59	54.95	786	761.52	708.85
5	40,000	8.38	30	30	56.6	47.18	800	799.31	789.52

shown in Table 4. As the predicted and experimental results are in reasonable agreement, it can be concluded that the developed analytical model is validated.

At spindle speed 40,000 rpm, 10 mm/min feed rate, and 50 μm cutting depth (run1), both of the predicted temperatures, $\Delta\overline{T}_{INRL}$ and the T_{tcp}, are around glass transition temperature, T_g, and at this temperature, fracture toughness is high [21] as shown in Fig. 6. The experimental results at these conditions, i.e., at spindle speed 40,000 rpm, feed rate 10 mm/min, and cutting depth 50 μm as shown in Fig. 7 confirmed that ductile chip produced, rolled uniformly and removed from the surface as cutting progress; hence, a clean final machined surface is produced. Run 2 showed similar results where the generated temperature was 520 °C, which is also around T_g. Hence, thermal softening occurred [19]. The viscous-plastic response releases the residual stress, hence fracture toughness increased [21]. Consequently, strength decreased and ductility of soda-lime glass increased [37].

Results from run 3, 4, and 5 confirm that the T_{tcm} is above T_g. The SEM view of machined surface and chip morphology showed that in those cases, molten chips are contaminated on the surface. In this regard, it can be stated that high speed and feed rate combinations are susceptible to produce molten chip. Figure 8 depicts that at spindle speed 30,000 rpm, 20 mm/min feed rate, and 40 μm cutting depth (run 3), low and high strain regions formed in the chip. Hence, thermal softening is not homogeneous throughout the removable layers of material; therefore, molten chips contaminated on the machined surface.

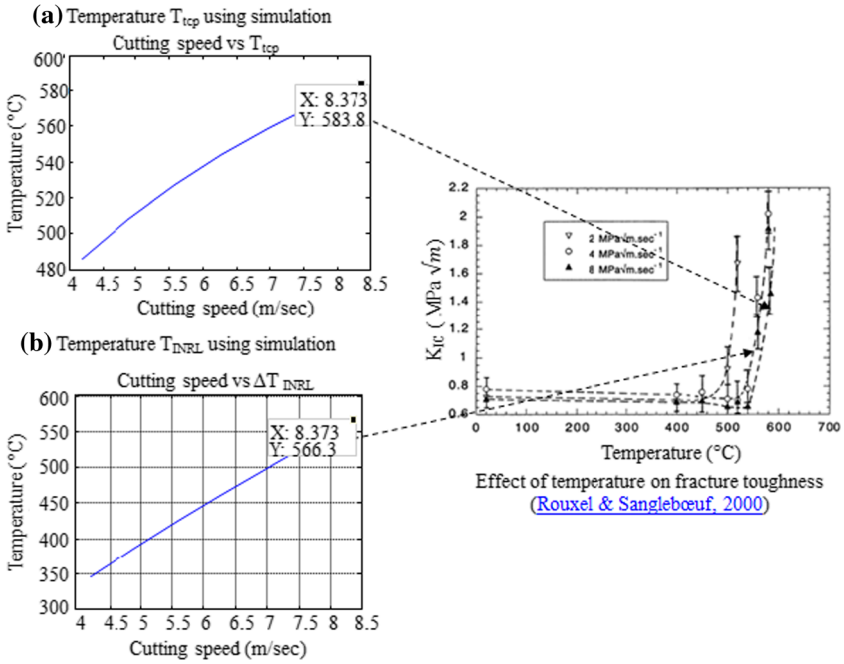

Fig. 6 The predicted $\Delta\overline{T}_{INRL}$ and the T_{tcp} are around glass transition temperatures of soda-lime glass

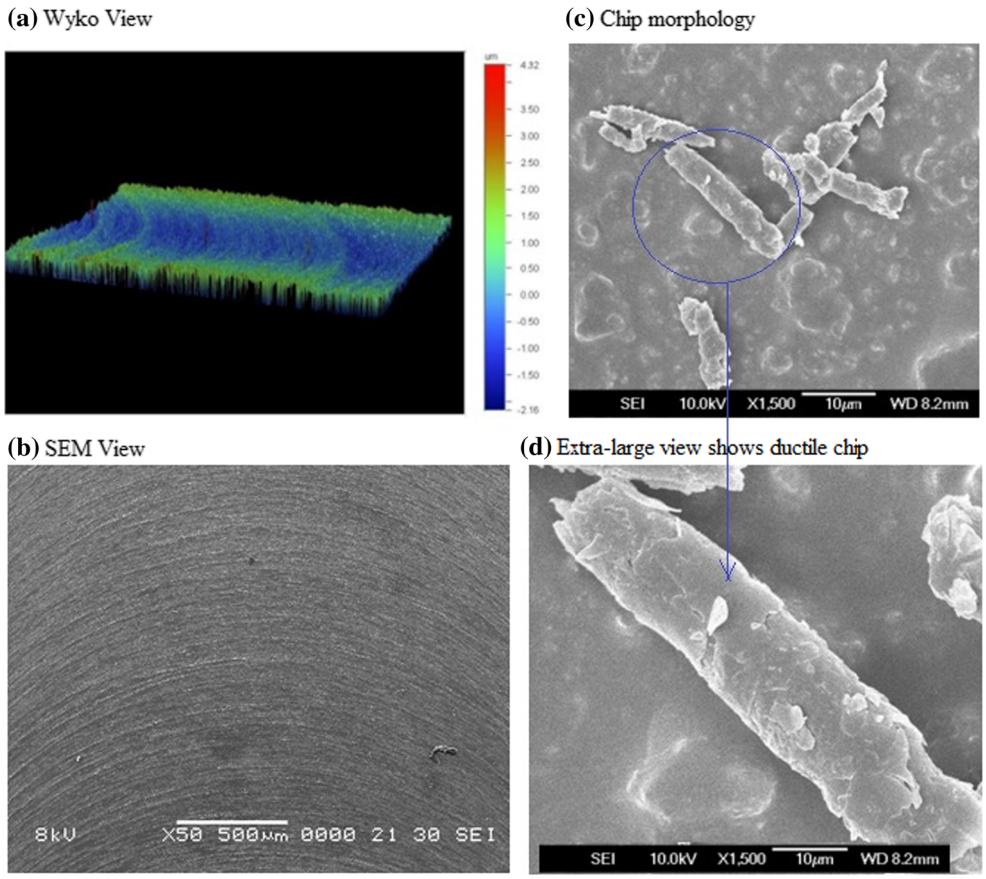

Fig. 7 End milling at 40,000 rpm (8.37 m/s), 10 mm/min feed rate, 0.13 μm/tooth, and 50 μm depth of cut generate temp. 587.56 °C while surface roughness R_a = 0.50 μm, R_t = 5.7 μm, and material removal rate 0.03 mm^3/s. **a** Wyko view. **b** SEM view. **c** Chip morphology. **d** Enlarged chip view

At 90° cutter rotation, uncut chip thickness is equal to feed per tooth [38] as shown in Fig. 2. At a constant feed rate with the increases of cutting speed feed per tooth decreases, hence uncut chip thickness decreases. Therefore, at a constant feed rate and cutting tool edge radius, the ratio of uncut chip thickness and cutting edge radius (t_1/r_e) decreases as cutting speed increased, hence amount of strain rate increased. This strain rate becomes as high as the order of 10^6. Also, negative rake angle and low value of shear angle brought high amount of strain on the machining point. Simulation results at 20 mm/min feed rate and cutting speed from 4.18 to 10.47 m/s (20,000 to 50,000 rpm) show that as strain rate increases, temperature $\Delta\overline{T}_{INRL}$ (°C) at the shear plane increases shown in Fig. 9.

The volume of removable layer tends to be large due to high value of UCT. Due to low thermal conductivity of glass and reduced strain rate, adiabatic flow is reduced at larger value of UCT; hence, as uncut chip thickness increases, temperature decreases as shown in Fig. 10. In high-speed milling, ductile mode coupled with thermal softening effect provides enhanced flexibility in DRM field. The combinations of cutting parameters and tool edge radius should be chosen which can generate temperature in the INRL around T_g. Using the analytical Eq. (14), this prediction is possible to achieve.

6 Conclusions

The developed analytical model can predict temperature generated in INRL of soda-lime glass based on fundamental micro-machining principle and material physical properties. The model incorporates the effects of cutting speed, feed rates, strain rate, material strength, and thermal softening effect. The following are some specific conclusions drawn from the study.

i. Simulation results showed that the relation between cutting tool edge radius and uncut chip thickness have significant effect on strain rate. At different cutting speed and feed rate, strain rate becomes as high as the order of 10^6. As strain rate increase, temperature at the shear plane increased.
ii. The model proved that high-speed cutting can generate adequate adiabatic heating, causing temperature rise in the INRL of work material around glass transition temperature. The simulation results carried

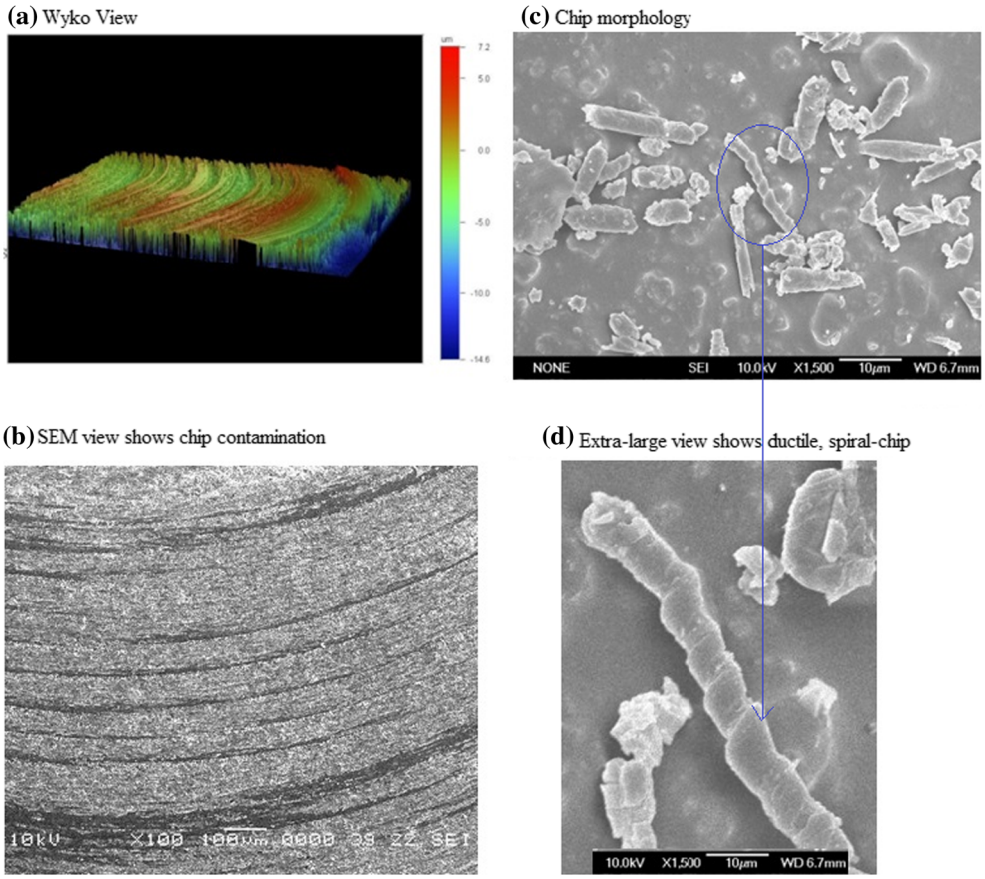

Fig. 8 End milling at 30,000 rpm (6.28 m/s), 20 mm/min feed rate, 0.33 μm/tooth, and 40 μm depth of cut generate temp 736 °C while produce $R_a = 1.66$ μm, $R_t = 13.89$ μm, and material removal rate 0.04 mm^3/s. **a** Wyko view. **b** SEM view. **c** Chip morphology. **d** Enlarged chip view

out at spindle speed 40,000 rpm, 10 mm/min feed showed that both of the temperature, $\Delta\overline{T}_{INRL}$ (566.33 °C) and the tool chip interface temperature, T_{tcp} (583.78 °C) is around glass transition temperature. Experimental verification of the tool chip interface temperature at 40,000 rpm, 10 mm/min feed rate and 50 μm depth also confirmed that temperature, T_{tcm} is 587.56 °C. At this temperature (glass transition temperature), ductile surface with low value of roughness was achieved.

iii. Above, the T_g molten chips are contaminated on the machined surface.

iv. The developed analytical model is also experimentally verified at different combinations of cutting parameters. As the predicted and experimental results are in reasonable agreement, hence the model is validated.

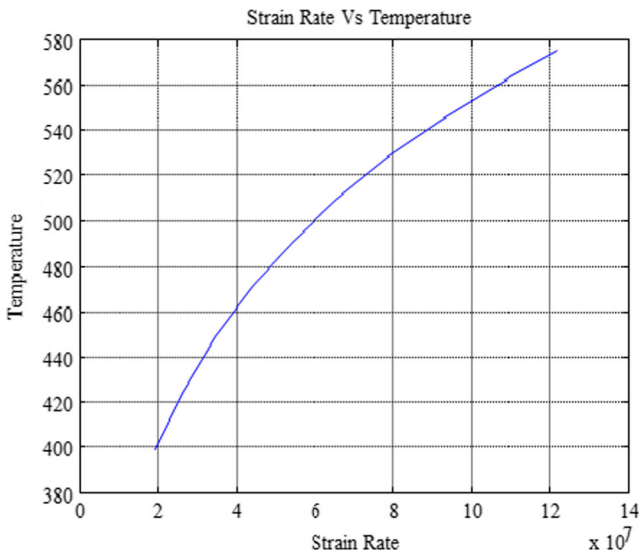

Fig. 9 Relation between strain rate and temperature

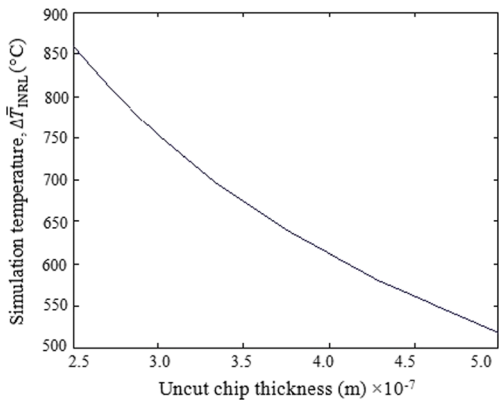

Fig. 10 Uncut chip thickness and temperature relation

Funding information The authors are grateful to the Fundamental Research Grant Scheme (FRGS14-120-0361) for funding this study.

References

1. Foy K et al (2009) Effect of tilt angle on cutting regime transition in glass micromilling. Int J Mach Tools Manuf 49(3):315–324
2. Smith, W.F. and J. Hashemi, Foundations of materials science and engineering. 2006: Mcgraw-Hill Publishing
3. Bifano, T.G., T.A. Dow, and R.O. Scattergood. Ductile-regime grinding of brittle materials: experimental results and the development of a model. In 32nd Annual Technical Symposium. 1989. International Society for Optics and Photonics
4. Arefin S et al The upper bound of tool edge radius for nanoscale ductile mode cutting of silicon wafer. Int J Adv Manuf Technol 2007, 31(7–8):655–662
5. Cai M, Li X, Rahman M (2007) Study of the mechanism of nanoscale ductile mode cutting of silicon using molecular dynamics simulation. Int J Mach Tools Manuf 47(1):75–80
6. Arif M, Rahman M, San WY (2011) Analytical model to determine the critical feed per edge for ductile–brittle transition in milling process of brittle materials. Int J Mach Tools Manuf 51(3):170–181
7. Zhao, Y., et al. An experimental investigation on the surface morphology in micro-end-milling of glass. In Automation and Computing (ICAC), 2014 20th International Conference on. 2014. IEEE
8. Moriwaki T, Shamoto E, Inoue K (1992) Ultraprecision ductile cutting of glass by applying ultrasonic vibration. CIRP Annals-Manufacturing Technol 41(1):141–144
9. Zhang X et al (2013) A model to predict the critical undeformed chip thickness in vibration-assisted machining of brittle materials. Int J Mach Tools Manuf 69:57–66
10. Lin S et al (2015) Application of ultrasonic assisted machining technique for glass-ceramic milling. World Academy Sci, Engineering Technol, Int J Mechanical, Aerospace, Industrial, Mechatronic Manufacturing Engineering 9(5):802–807
11. Rao DMS, Shrekanth D (2014) Abrasive jet machining-research review. Int J Advanced Engineering Technol 5:18–24
12. Aich U et al (2014) Abrasive water jet cutting of borosilicate glass. Procedia Materials Sci 6:775–785
13. Jui SK, Kamaraj AB, Sundaram MM (2013) High aspect ratio micromachining of glass by electrochemical discharge machining (ECDM). J Manuf Process 15(4):460–466
14. Mohammadi H et al (2015) Experimental work on micro laser-assisted diamond turning of silicon (111). J Manuf Process 19: 125–128
15. Wlodarczyk KL et al (2016) Picosecond laser cutting and drilling of thin flex glass. Opt Lasers Eng 78:64–74
16. Sajjadi, M., et al. Investigation of micro scratching and machining of glass. In ASME 2009 International Manufacturing Science and Engineering Conference. 2009. American Society of Mechanical Engineers
17. Reddy, M.M., A. Gorin, and K. Abou-El-Hossein. Predictive surface roughness model for end milling of machinable glass ceramic. In IOP Conference Series: Materials Science and Engineering. 2011. IOP Publishing
18. Amin A et al (2016) An experimental approach to determine the critical depth of cut in brittle-to-ductile phase transition during end milling of soda-lime glass. Arab J Sci Eng 41(11):4553–4562
19. Le Bourhis E, Metayer D (2000) Indentation of glass as a function of temperature. J Non-Cryst Solids 272(1):34–38
20. Michel M et al (2004) High temperature microhardness of soda-lime glass. J Non-Cryst Solids 348:131–138
21. Rouxel T, Sanglebœuf J-C (2000) The brittle to ductile transition in a soda–lime–silica glass. J Non-Cryst Solids 271(3):224–235
22. Johnson, G.R. and W.H. Cook. A constitutive model and data for metals subjected to large strains, high strain rates and high temperatures. In Proceedings of the 7th International Symposium on Ballistics. 1983. The Hague, The Netherlands
23. Rao S, Shunmugam M (2012) Analytical modeling of micro end-milling forces with edge radius and material strengthening effects. Mach Sci Technol 16(2):205–227
24. Srinivasa Y, Shunmugam M (2013) Mechanistic model for prediction of cutting forces in micro end-milling and experimental comparison. Int J Mach Tools Manuf 67:18–27
25. Venkatachalam S et al (2015) Microstructure effects on cutting forces and flow stress in ultra-precision machining of polycrystalline brittle materials. J Manuf Sci Eng 137(2):021020
26. Venkatachalam S, Li X, Liang SY (2009) Predictive modeling of transition undeformed chip thickness in ductile-regime micro-machining of single crystal brittle materials. J Mater Process Technol 209(7):3306–3319
27. Oxley, P., The mechanics of metal cutting. An analytical approach to assessing machinability. 1989, Chichester, Elis Horwood Limited
28. Altintas, Y., Mechanics of metal cutting. Manufacturing automation: metal cutting mechanics, machine tool vibrations, and CNC design, Cambridge, UK. Cambridge University Press, 2000: p. 4–65
29. Zhou L et al (2015) Analytical modeling and experimental validation of micro end-milling cutting forces considering edge radius and material strengthening effects. Int J Mach Tools Manuf 97:29–41
30. Boothroyd, G. and Ey, Temperatures in orthogonal metal cutting. Proceedings Institution Mechanical Engineers, 1963. 177(1): p. 789–810
31. Lazoglu I, Altintas Y (2002) Prediction of tool and chip temperature in continuous and interrupted machining. Int J Mach Tools Manuf 42(9):1011–1022
32. Callister, W.D. and D.G. Rethwisch, Materials science and engineering. Vol. 5. 2011: John Wiley & Sons NY
33. Zhang X, Hao H, Ma G (2015) Dynamic material model of annealed soda-lime glass. Int J Impact Eng 77:1088–1119
34. Callister, W.D. and D.G. Rethwisch, Materials science and engineering: an introduction. Vol. 7. 2007: Wiley New York
35. Holmquist TJ, Johnson GR (2011) A computational constitutive model for glass subjected to large strains, high strain rates and high pressures. J Appl Mech 78(5):051003
36. Zhang X, Hao H, Ma G (2015) Dynamic material model of annealed soda-lime glass. Int J Impact Engineering 77:108–119
37. Nie X et al (2009) Effect of loading rate and surface conditions on the flexural strength of borosilicate glass. J Am Ceram Soc 92(6): 1287–1295
38. Lee HU, Cho D-W, Ehmann KF (2008) A mechanistic model of cutting forces in micro-end-milling with cutting-condition-independent cutting force coefficients. J Manuf Sci Eng 130(3): 031102